Molybdenum disulfide (MoS_2) -based cathode materials for magnesium (Mg^{2+}) and Mg^{2+}/Li^+ hybrid-ion batteries: Progress and perspective

Falyouna, Omar
Center for Advanced Battery Collaboration, Research Center for Energy and Environmental Materials, National Institute for Materials Science

Mandai, Toshihiko
Center for Advanced Battery Collaboration, Research Center for Energy and Environmental Materials, National Institute for Materials Science

https://doi.org/10.5109/7157941

出版情報：Proceedings of International Exchange and Innovation Conference on Engineering & Sciences (IEICES). 9, pp.34-42, 2023-10-19. 九州大学大学院総合理工学府
バージョン：

Molybdenum disulfide (MoS_2)−based cathode materials for magnesium (Mg^{2+}) and Mg^{2+}/Li^{+} hybrid-ion batteries: Progress and perspective

Omar Falyouna[1*] and Toshihiko Mandai[1*]
[1] Center for Advanced Battery Collaboration, Research Center for Energy and Environmental Materials, National Institute for Materials Science, 1-1 Namiki, Tsukuba, Ibaraki, 305-0044, Japan
*Corresponding author email: FALYOUNA.Omar@nims.go.jp & MANDAI.Toshihiko@nims.go.jp

Abstract: *Rechargeable magnesium batteries (RMBs) are gaining a great deal of attention as a promising alternative for lithium-ion batteries (LIBs) because of the distinctive properties of Mg such as abundant sources in nature, large theoretical capacity, stability of bulk metal against the ambient atmosphere, etc. However, the development of RMBs is still in the early stages, especially on the cathode side. RMBs with intercalation-type cathodes often suffer from sluggish kinetics due to the high polarization of the divalent Mg^{2+}. Molybdenum disulfide (MoS_2) is a layered transition metal dichalcogenide and serves as a prospective base material for Mg^{2+} intercalation. This mini-review summarizes the state-of-the-art in the development of MoS_2−based cathode materials for RMBs and Mg^{2+}/Li^{+} hybrid ion batteries (MLIBs).*

Keywords: Rechargeable magnesium battery (RMBs); Hybrid Mg^{2+}/Li^{+} ion battery; Molybdenum disulfide (MoS_2).

1. INTRODUCTION

Lithium-ion batteries (LIBs) are widely utilized in the market as excellent energy storage technologies, especially for portable electronic devices, because of their high energy density and exceptional durability [1]. However, the scarcity of lithium resources (i.e., 0.0017% by weight in the earth's crust) significantly increases the cost of LIBs [2]. Moreover, the utilization of flammable electrolytes and the formation of dendritic depositions impose many serious operational safety issues which hinder their further development, particularly for industrial−scale applications (e.g., e−transportation, energy grid storage systems, etc.) [3].

On the other hand, rechargeable magnesium batteries (RMBs) are promising alternatives for energy storage and conversion applications owing to their unique electrochemical characteristics such as remarkable theoretical capacity (i.e., 2205 mAh g^{-1} and 3833 mAh cm^{-3}), low electrode potential (−2.36 V vs. standard hydrogen electrode), the high elemental abundance of magnesium in the earth's crust (24.31% by weight), reasonable cost, and environmentally friendliness [2], [4]. In addition, unlike Li anodes, Mg metal anodes are chemically stable and don't form dendrites under normal electrochemical reactions which remarkably improves the operational safety of RMBs [5].

Nevertheless, the development of RMBs is still facing several challenges and issues. For instance, Mg^{2+} intercalation/deintercalation into/from the interlayer spacing of various cathode materials is kinetically sluggish due to the high energy barrier of Mg^{2+} diffusion [2], [6]. Moreover, the Mg metal anode and conventional carbonate-based electrolytes are incompatible because of the strong polarization nature of Mg^{2+} cations [7], [8]. These shortcomings severely deteriorate the capacity, rate capability, and cycling ability of RMBs. Hence, it is crucial to develop a cathode material with high affinity to easily insert/extract Mg^{2+}, an anode with less passivation, and a highly stable electrolyte to promote the electrochemical performance of RMBs.

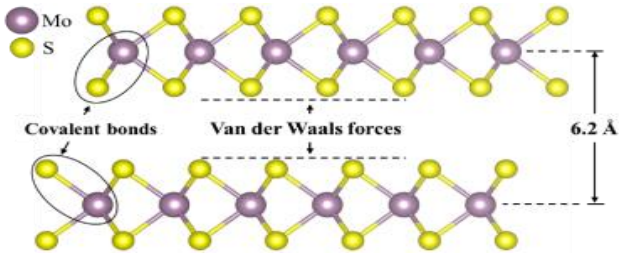

Fig. 1. Two-dimensional structure of MoS_2 [9].

Over the past years, researchers have made great efforts to propose suitable cathode materials for RMBs such as titanium disulfide nanotubes (TiS_2) [10], layered manganese dioxide (MnO_2) [11], vanadium(V) oxide nanotubes (V_2O_5) [12], MXenes [13], cobalt sulfide (CoS) spheres [14], and so forth. Among these materials is molybdenum disulfide (MoS_2), a well-known layered transition metal dichalcogenide (TMD) with a graphene−like structure [15]. It is an ideal candidate as an active cathode material for RMBs because of its unique structure where two sulfur (S) layers are separated by a molybdenum (Mo) layer and stacked all together by van der Waals forces (F_{VW}) as shown in **Fig. 1** [9], [15]. The flexibility of MoS_2 allows the smooth insertion and extraction of Mg^{2+} cations during the discharge and charge processes [16]. This review is dedicated to shedding light on the recent development of MoS_2−based composites as cathode materials in RMBs and Mg^{2+}/Li^{+} hybrid-ion batteries (MLIBs). The electrochemical performance of MoS_2−based composites was summarized based on the initial specific capacity, cyclic capacity, and number of cycles under different battery configurations as presented in **Table *1*** and **2**.

2. WORKING PRINCIPLE OF RMBs

RMBs are storage devices that transform chemical energy into electrical energy through an electrochemical reaction [2]. They consist of three main parts, namely anode, cathode, and electrolyte (**Fig. 2**) [17]. The anode composes of pure Mg or Mg alloys and acts as a reductant (**Eq. 1**). While the cathode acts as an oxidant and comprises a chemically stable material that is capable of a reversible insertion/extraction of Mg^{2+} such

as MoS_2 (**Eq. 2**). Also, as displayed in **Fig. 2**, the cathode and anode are separated by a permeable membrane to prevent their direct contact and only permits the free movement of Mg^{2+} [6].

$$\text{Anode} \quad 4Mg \leftrightarrow 4Mg^{2+} + 8e^- \quad (1)$$

$$\text{Cathode} \quad 6MoS_2 + 4Mg^{2+} \leftrightarrow Mg_4Mo_6S_{12} \quad (2)$$

$$\text{Overall} \quad 4Mg + 6MoS_2 \leftrightarrow Mg_4Mo_6S_{12} \quad (3)$$

During the discharge Mg metal will undergo an oxidation reaction to release Mg^{2+} and electrons (**Eq. 1**) [4], [17]. Then, Mg^{2+} will diffuse in the electrolyte and migrate to the cathode side. After reaching the cathode, Mg^{2+} will intercalate in the interlayer spacing of MoS_2 (**Fig. 2** & **Eq.2**). On the contrary, on charging, Mg^{2+} will be deintercalated from MoS_2 and moves back toward the anode (**Fig. *2***) [6]. Throughout the discharge/charge cycles, electrons will transfer *via* the external circuit to balance the charge between the electrodes (**Fig. 2**) [2].

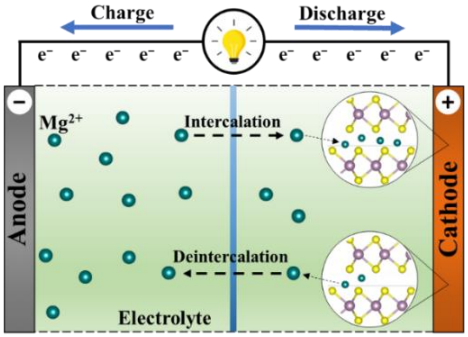

Fig. 2. Schematic diagram of RMB cell.

3. RMB with MoS_2−based cathode

The literature survey revealed that *sixteen research articles*, with a focus on the application of MoS_2−based materials as a cathode material for RMBs, were published between 2004 and 2023 (**Fig. *3*.a**).

MoS_2 is used to be synthesized by utilizing many reductants, for example, H_2S, $NaBH_4$, SO_2, etc. at high temperatures (e.g., 850 ℃) [18]. In contrast, Li *et al.* demonstrated that MoS_2 nanostructures could be prepared by using sulfur compounds as reductants at moderate temperatures [18]. They emphasized that sulfurization compounds will decompose at temperatures higher than 150 ℃ in acidic solutions to form H_2S which is used to reduce Mo(VI) (**Eq. 4**).

$$Na_2S + 2HCL \rightarrow 2NaCl + H_2S \quad (4)$$

Using several sulfurization compounds, e.g., CS_2, KSCN, CH_3CSNH_2, Na_2S, CSN_2H_4, in a hydrothermal process at 180 ℃, they managed to obtain various nanostructures of MoS_2 namely, spherical nanovesicles, hollow-cage fullerene-like structures, and fibrous floccus [18]. They investigated the Mg^{2+} intercalation/deintercalation ability of as-prepared MoS_2 and they found that these materials could deliver a cell capacity ranging between 2 and 25 mAh g^{-1} at 0.02 mA g^{-1} (**Table *1***). Liang *et al.* followed the same procedures to synthesize graphene-like MoS_2 (G−MoS_2) *via* a solvothermal reaction between MoO_3 and thioacetamide while being mixed in pyridine at 150 ℃ [4]. The as-synthesized G−MoS_2 was then used as a cathode material and magnesium nanoparticles (N−Mg) as an anode in RMBs. The fabricated [G-MoS_2|$Mg(AlCl_3Bu)_2$/THF|N−Mg] cell exhibited an excellent reversible specific capacity of 170 mAh g^{-1} at 20 mA g^{-1} (**Table 1**). 95% of the initial specific capacity of G−MoS_2 was obtained after 50 cycles whereas the Columbic efficiency was approximately 99% (**Table 1**). These results clearly state that simple modification in the synthesis process will substantially affect the electrochemical activity of MoS_2 in RMBs. Yang *et al.* estimated the maximum theoretical capacity of zigzag MoS_2 nanoribbon via density functional theory (DFT) calculations [16]. They declared that a maximum capacity of 223.2 mAh g^{-1} could be theoretically achieved due to the double-side Mg adsorptions. Since the maximum theoretical capacity of MoS_2 hadn't been reached yet, various enhancement techniques have been applied to improve the electrochemical performance of MoS_2 such as carbon coating, expansion of interlayer spacing, ion introduction, defect engineering, crystal water intercalation, and so on [2], [6].

3.1 Carbon Coating/Supportation

It has been reported that carbon coating is an effective method to improve the electrochemical performance of MoS_2 by not only improving the electric conductivity and accelerating the transfer of charge but also by providing a framework that helps in reducing the volume change throughout the discharge/charge reactions [2], [19]. For example, Liu *et al.* coated MoS_2 with a carbon material by adding different weights of glucose, as a carbon source, during the hydrothermal process to formulate MoS_2/C microspheres [19]. MoS_2/C, with a carbon content of 46 wt%, showed a remarkable specific capacity of 213 mAh g^{-1} with a cycling capacity of 84.3 mAh g^{-1} after 50 cycles (**Table 1**). This improvement was ascribed to the enhancement in the electrical conductivity of the MoS_2/C cathode as the electrochemical impedance spectra measurements indicated that the overall resistance of the battery significantly reduced after incorporating carbonaceous materials in MoS_2. On another two occasions, Liu *et al.* replaced the carbonaceous material, which resulted from glucose carbonization, with reduced graphene oxide (MoS_2−rGO) [20] and graphene (MoS_2/G) [8] to support MoS_2 and promote the electrochemical performance of RMBs. They manifested that the existence of a graphene layer within the MoS_2 structure not only expanded the interlayer spacing (i.e., from 0.62 to 0.98 nm in the case of MoS_2/G [8]) but also prevented the stacking of MoS_2 layers and provided a good platform for MoS_2 to grow with less aggregation [8], [20]. Although graphene intercalation in MoS_2 facilitated the interfacial charge transfer and enhanced the electric conductivity, MoS_2−rGO and MoS_2/G−15 (i.e., 15 mg of graphene was added during the hydrothermal process) provided a moderate specific capacity of 104.2 and 115.9 mAh g^{-1}, respectively (**Table *1***). Conversely, Wu *et al.* presented a promising technique to synthesize van der Waals' heterostructures (vdWHs) by sandwiching a graphene layer (GR) between two layers of MoS_2 to synthesize MoS_2/GR [21]. The outcomes of the electrochemical analysis declared that the MoS_2/GR delivered an outstanding specific capacity of 210 mAh g^{-1} with an excellent cycling capacity of 182.7 mAh g^{-1} after 300 cycles at 20 mA g^{-1} (**Table 1**). The excellent performance of MoS_2/GR, compared to MoS_2−rGO and MoS_2/G−15 (**Fig. *3*.a**), was attributed to the successful intercalation of graphene between MoS_2 layers which notably expanded the interlayer distance from 0.62 to 1.16 nm.

This layer expansion greatly enhanced the diffusivity of Mg^{2+} in MoS_2/GR (i.e., 3.24×10^{-9} cm^2 S^{-1}) eleven times more than that of bulk MoS_2 (i.e., 10^{-20} cm^2 S^{-1}) and reduced the diffusion energy barrier to 0.4 eV.

3.2 Interlayer Expansion

Previous reports indicated that the interlayer spacing between the layers of MoS_2 is approximately 0.62 nm (**Fig. *1***) [8], [21], [22]. As stated in the previous section, expanding the interlayer spacing of MoS_2 can improve the insertion/extraction of Mg^{2+} by reducing the diffusion energy barrier [6], [22]. Instead of using graphene, Liang *et al.* adopted a different technique to expand the interlayer spacing by inserting certain amounts of poly(ethylene oxide) (PEO) between the layers of MoS_2 (PEO−MoS_2) [22]. Their technique managed to enlarge the interlayer spacing from 0.62 to 1.45 nm (i.e., more than MoS_2/GR [21]) by intercalating PEO with a MoS_2:PEO molar ratio of 1:1 (peo_2−MoS_2). Although the huge interlayer expansion by PEO is beneficial to accelerate the diffusion kinetics of Mg^{2+} in MoS_2, only less than 75 mAh g^{-1} by peo_2−MoS_2 could be delivered definitely due to the inclusion of large amounts of inactive components (**Table 1**). Wu *et al.* obtained an interlayer spacing of 0.97 nm by inserting polyvinylpyrrolidone (PVP) into the layered structure of MoS_2 (PVP−MoS_2) [5]. The diffusivity coefficient of Mg^{2+} in PVP−MoS_2 considerably increased by 51 orders of magnitude compared with the bulk MoS_2. PVP−MoS_2 exhibited a good initial specific capacity of 143.4 mAh g^{-1} at 20 mA g^{-1} (**Table 1**). Also, the cycling experiments proved that PVP helped MoS_2 to maintain the layered structure during the cycling process as 92% of the initial capacity was achieved after 100 cycles.

3.3 Ion Introduction

The sluggish diffusion of Mg^{2+} in the interlayer spacing of MoS_2 is mainly caused by the divalent nature of Mg^{2+} [23], [24]. However, the pre-introduction of ion/ions (e.g., cations or anions) could enhance the diffusion kinetics of Mg^{2+} by shielding the effect of the strong charge of Mg^{2+} during the intercalation/deintercalation in MoS_2 [2], [15], [25]. Venkateswarlu *et al.* demonstrated that fluorination of MoS_2 (F−MoS_2) enhanced the electrochemical performance of bulk MoS_2 (B−MoS_2) from approximately 39 to nearly 55 mAh g^{-1} at 15 mA g^{-1} (**Table 1**) [26]. The electrochemical impedance spectroscopy (EIS) of B−MoS_2 and F−MoS_2 indicated that the electrochemical enhancement resulted from increasing the conductivity of F−MoS_2|Mg cell after F−doing (i.e., R_{SEI}: 500 Ω → 400 Ω and R_{ct}: 1400 Ω → 1100 Ω). Also, Zhuo *et al.* reported that Cu−MoS_2 achieved a better specific capacity of 150 mAh g^{-1}, compared to pristine MoS_2 (i.e., less than 100 mAh g^{-1} at 50 mA g^{-1}) [25]. Unfortunately, the electrochemical efficiency of Cu−MoS_2 gradually decreased as the cycling number increased to finally achieve around 91 mAh g^{-1} after 200 cycles. On the other hand, when Cu−MoS_2 was supported by hydrogen-substituted graphdiyne nanotubes (HsGDY) to form Cu−MoS_2@HsGDY nano−capsules, the specific capacity of Cu−MoS_2@HsGDY was preserved even after 200 cycles (i.e., 150 mAh g^{-1} declined to 148.5 mAh g^{-1} after 200 cycles) (**Table 1**). The expanded interlayer spacing and the abundant active sites of Cu−MoS_2 facilitated the diffusion of Mg^{2+}. While the HsGDY prevented the restacking and aggregation of Cu−MoS_2. The mutual effect of the structure's components uniquely promoted the electrochemical performance of Cu−MoS_2@HsGDY in RMBs. The findings of Zhuo *et al.* [25] reflect the importance of the supporting material to enhance the cycling ability of MoS_2−based materials.

3.4 Defect Engineering/Modification

Defect engineering is another strategy to modify the surface properties and improve the electrochemical performance of MoS_2 in multivalent rechargeable batteries [2], [15]. There are two types of defects: intrinsic and non-intrinsic [15]. Intrinsic defects, e.g., Schottky defects, are internal defects generated via thermal vibration of the atomic lattice without changing the composition of the crystal [15]. In contrast, non-intrinsic defects, also known as heteroatomic defects, are created by inserting ions in the interlayer spacing of MoS_2 [15]. Zhu *et al.* tried to create a defective MoS_2 structure by changing the Mo:S ratio, such as 1:2, 1:4, and 1:7, during the thermal synthesis of MoS_2 nanosheets [27]. MoS_2 nanosheets with a Mo:S ratio of 1:7 exhibited a neglectable electrochemical performance and were excluded from the comparison. Whereas MoS_2 with Mo:S of 1:2 and 1:4 showed a poor initial specific capacity of approximately 20 and 25 mAh g^{-1}, respectively. However, MoS_2 with Mo:S of 1:2 and 1:4 needed 141 and 41 cycles, respectively, to reach their maximum specific capacity of 67 and 152 mAh g^{-1} (**Table 1**). After reaching their maximum specific capacity, the specific capacity of both defective MoS_2 nanosheets decreased to approximately 75 and 20 mAh g^{-1}, after increasing the number of cycles to 200 and 100, respectively. It is hard to control the formation of defects during the synthesis process and the misapplication of this technique may cause serious failures in the structure of MoS_2 [15]. Therefore, further research on the proper use of defect engineering for MoS_2−based materials is needed.

3.5 Crystal water incorporation

The insertion of H_2O molecules into the interlayer spacing of MoS_2 facilitates the diffusion of Mg^{2+} by shielding the charge effect of the divalent Mg^{2+} [2], [28]. Wu *et al.* investigated the impact of H_2O intercalation on the electrochemical activity of the synthesized oxygen−doped MoS_2 (O−MoS_2) in RMBs [29]. They stated that O−MoS_2 was in the 1T phase with an enlarged interlayer spacing of 0.94 nm. The special structure of O−MoS_2, compared with the pristine MoS_2, favors the intercalation of Mg^{2+} with an initial specific capacity of 130.2 mAh g^{-1}. This excellent performance was further promoted to 190.3 mAh g^{-1} after MoS_2 hydration (H−MoS_2) via an electrochemically assisted procedure (**Table 1**). XRD and SEM analysis confirm that MoS_2 hydration further enlarged the interlayer spacing from 0.92 nm to 1.03 nm. Also, the EIS analysis and the galvanostatic intermittent titration technique (GITT) proved that water intercalation accelerated the diffusivity of Mg^{2+} in H−MoS_2 (i.e., 1.41×10^{-9} cm^2 S^{-1}), four and eleven times faster than that of O−MoS_2 and pristine MoS_2 (i.e., 10^{-20} cm^2 S^{-1}), respectively. Also, the cyclic voltammetry analysis indicated that MoS_2 hydration not only boosted the electrochemical performance of O−MoS_2 but also promoted the capacity retention from 44% (O−MoS_2) to nearly 91% (H−MoS_2) after 300 cycles (**Table 1**).

Table 1. Electrochemical performance of various MoS_2−based cathode materials under different configurations of RMBs.

Battery Configuration				Electrochemical performance						Ref.
Cathode Material	**Anode Material**	**Electrolyte**	**Separator**	**Current density (mA g^{-1})**	**Temp. (°C)**	**Voltage window (V *vs.* Mg/Mg^{2+})**	**Initial specific capacity (mAh g^{-1})**	**Cyclic capacity (mAh g^{-1})**	**No. of cycles**	
MoS_2	Mg flakes	$Mg(AlCl_3Bu)_2$/THF	Cellgard 2400	0.02	Room Temp.	0.6−2.8	25	–	–	[18]
MoS_2 (G−MoS_2)	Mg nanoparticles	$Mg(AlCl_3Bu)_2$/THF	Celgard	20	–	0.0−3.0	170	168.3	50	[4]
MoS_2 Nanoribbon	–	–	–	–	–	–	223.2	–	–	[16]
MoS_2/C microspheres (Carbon content: 46 wt%)	AZ31 Mg alloy	0.4 M $Mg_2Cl_3^+ \cdot AlPh_2Cl_2^-$/THF	Celgard 2320	50	Room Temp.	0.0−2.2	213	84.3	50	[19]
MoS_2−rGO	AZ31 Mg alloy	0.4 M $Mg_2Cl_3^+ \cdot AlPh_2Cl_2^-$/THF	Celgard 2320	20	Room Temp.	0.0−2.2	104.2	74.1	50	[20]
MoS_2−PEO (peo_2−MoS_2)	Polished Mg foil	0.25 M APC/THF	–	5	Room Temp.	0.2−2.0	75	70	30	[22]
MoS_2/G−15	AZ31 Mg alloy	0.4 M $(PhMgCl)_2{}^-AlCl_3$/THF	Celgard 2320	20	25	0.0−2.2	115.9	82.5	50	[8]
MoS_2/MXene	Mg disc	APC electrolyte	Polypropylene membranes	50	–	0.01−2.0	165	108	50	[7]
F−MoS_2	Mg powder	0.5M $Mg(ClO_4)_2$ in [*bim*][Br]	Celgard	15	–	0.3−2.5	55	40	50	[26]
PVP−incorporated MoS_2	Mg metal	0.25 M APC/ THF	Celgard 2400	20	–	0.2−2.0	143.4	131.9	100	[5]
MoS_2-infilled microcapsule	AZ31 Mg alloy	0.4 M APC/THF	Glass fiber filter	50	–	0.01−2.2	161	100	100	[30]
Defective MoS_2 nanosheets	Mg tablets	$[Mg_2Cl_3]^+ \cdot [AlPh_2Cl_2]^-$/THF (APC)	Whatman GF/B	20	–	0.2−2.2	30	75	100	[27]
MoS_2@carbon@ polyaniline	AZ31 Mg alloy	0.4 M $(PhMgCl)_2$-$AlCl_3$/THF	–	100	–	0.01−2.0	127	114	100	[31]
MoS_2/GR	Mg metal	0.25 M APC/THF	Celgard 2400	20	–	0.2−2.0	210	182.7	300	[21]
Hydrous MoS_2 (H−MoS_2)	Mg metal	0.25 M of APC electrolyte/THF	Celgard 2400	20	–	0.2−2.2	190.3	173.55	300	[29]
Cu−MoS_2@HsGDY	Mg metal foil	0.25 M of $MgCl_2$ and $AlCl_3$ (1:2 mol ratio) in DME	Whatman glass fibers	50	–	0.1−2.2	148.5	148.5	200	[25]

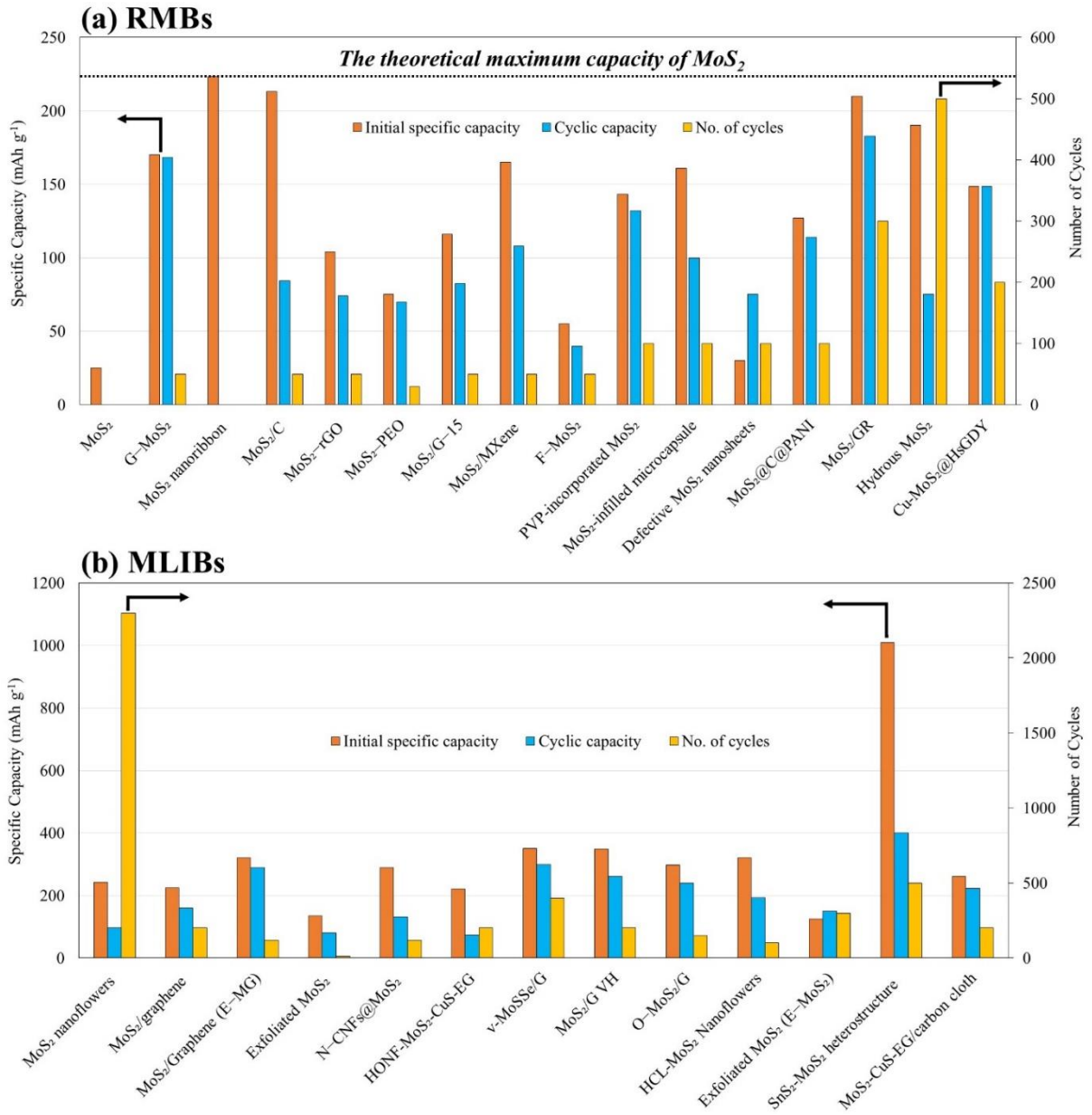

Fig. 3 Comparison between the electrochemical capacity of MoS_2−based cathode materials in (a) RMBs and (b) MLIB.

4. Mg^{2+}/Li^{+} HYBRID-ION BATTERY (MLIB)

Fig. 3.a epitomizes the electrochemical competence of sixteen different MoS_2−based materials in RMBs. Despite the appreciated efforts to promote the electrochemical ability of MoS_2, **Fig. 3.a** displays that few materials were able to nearly achieve the maximum theoretical capacity of MoS_2 (223.2 mAh g^{-1}) such as MoS_2/C (213 mAh g^{-1}), MoS_2/GR (210 mAh g^{-1}), and hydrous MoS_2 (190.3 mAh g^{-1}). In addition, the excellent performance of these materials faded as the number of discharge/charge cycles increased. These conclusions confirm the difficult and sluggish intercalation/deintercalation of Mg^{2+} in the interlayer spacing of MoS_2 even after the application of certain improvement techniques.

A group of researchers adopted a new approach to tackle the sluggish insertion of Mg^{2+} by fabricating Mg^{2+}/Li^{+} hybrid ion batteries (MLIBs) [1], [3], [40], [41], [32]–[39]. The components of MLIBs are the same as RMBs except for the utilization of dual-salt electrolytes (Mg^{2+}/Li^{+}) [33]. The unique configuration of MLIBs combines the benefit of using the dendrite-free Mg anode and the fast intercalation kinetics of Li^{+} which greatly enhances the reaction kinetics and magnifies the electrochemical performance of MLIBs. There are two types of MLIBs: Daniell−type battery and rocking−chair battery [1], [38]. In Daniell batteries, Li^{+} ions are solely intercalating in the interlayer spacing of the cathode materials [39]. Conversely, in rocking−chair batteries, both Mg^{2+} and Li^{+} are simultaneously inserted/extracted in/from the interlayer spacing of the cathode material during the discharge/charge cycles [1]. **Table *2*** and **Fig. 3.b** summarize the electrochemical efficiency of different MoS_2−based cathode materials in MLIBs. **Fig. 3** (a & b) highlights the superiority of MLIBS over RMBs as **Fig. 3.b** shows that most of the applied MoS_2−based cathodes in MLIBS exhibited exceptional specific capacities higher than the maximum theoretical capacity of MoS_2 in RMBs. For example, when Yanming Ju *et al.* employed MoS_2 nanoflowers as a cathode material in a dual−salt electrolyte of 1 M LiCl + 0.4 M APC/THF, the battery cell achieved a good initial specific capacity of 243 mAh g^{-1} (**Table *2***) [1].

Table 2. Electrochemical performance of various MoS_2−based cathode materials under different configurations of MLIBs.

Battery Configuration						Electrochemical performance				Ref.
Cathode Material	**Anode Material**	**Electrolyte**	**Separator**	**Current density (mA g^{-1})**	**Temp. (°C)**	**Voltage Window (V *vs.* Mg/Mg^{2+})**	**Initial specific capacity (mAh g^{-1})**	**Cyclic capacity (mAh g^{-1})**	**No. of cycles**	
MoS_2 nanoflowers	Mg foil	1 M LiCl + 0.4 M APC/THF	−	20	−	0.01−2.0	243	96.4[a]	2300	[1]
MoS_2/graphene	Mg foil	0.5 M LiCl + APC/THF	Glassy fiber membrane	25	25	0.1−1.8	225	160	200	[32]
MoS_2/Graphene foam	Metallic Mg ribbon	0.25 M LiCl + 0.25 M APC/THF	Celgard 3501	20	−	0.01−2.0	320	290	120	[33]
Exfoliated MoS_2	Mg metal	0.4 M LiCl + 0.4 M APC	Microporous polypropylene film	20	−	0.2−2.2	135	81	10	[34]
N−CNFs@MoS_2	Mg foil	84 mg LiCl + APC/THF	Whatman glass fiber paper	200	Room Temp.	0.01−1.8	290	131	120	[35]
HONF−MoS_2−CuS−EG	Mg foil	0.4 M LiCl + 0.4 M APC/THF	−	50	−	0.01−2.0	221.55	73.5	200	[3]
v−MoSSe/G	Mg plate	1.696 g LiCl + APC/THF	Celgard 2400	20	−	0.2−2.0	350.8	299.2	400	[37]
MoS_2/G VH	Mg plate	1.696 g LiCl + APC/THF	Celgard 2400	20	−	0.2−2.0	348.3	260.8	200	[42]
O−MoS_2/G	Mg plate	1.696 g LiCl + APC/THF	Celgard 2400	20	−	0.2−2.0	298.1	239.4	150	[38]
HCL-MoS_2 Nanoflowers	Mg metal	1 M LiCl + 0.4 M APC/THF	Glass fiber	100	−	0.01−2.0	321	192.8	100	[39]
Exfoliated MoS_2 (E−MoS_2)	Mg foil	0.8 M LiCl + APC/THF	Polypropylene film	100	Room Temp.	0.01−2.0	125	150	300	[40]
SnS_2−MoS_2 heterostructure	Mg ribbon	0.25 M LiCl + 0.25 MAPC/THF	Celgard 3501	50	−	0.01−2.0	1009	450	500	[41]
MoS_2-CuS−EG/carbon cloth	Mg foil	0.4 M LiCl + 0.4 M APC/THF	−	50	−	0.01−2.0	261.1	222.9	200	[36]

[a] The cyclic capacity of 96.4 mAh g^{-1} was attained at 1000 mA g^{-1}.

Xiong *et al.* further improved the electrochemical competence of MoS_2 by adding hydrochloric acid (HCL) to control the pH of the mixture of ammonium molybdate tetrahydrate and thiourea at 0.9 before starting the hydrothermal treatment at 220 ℃ [39]. The HCL−assisted synthesized MoS_2 attained a remarkable specific capacity of 321 mAh g^{-1} with a cyclic capacity of 192.8 mAh g^{-1} after 100 cycles (**Table *2***). On the contrary, the exfoliated MoS_2 proposed by Truong *et al.* [34] and Li *et al.* [40] showed poor electrochemical performance in MLIBs with s specific capacity of 135 and 125 mAh g^{-1}, respectively (**Table *2*** & **Fig. 3.b**). Similar to RMBs, many MoS_2−based composites were developed and applied as cathode materials to boost the electrochemical performance of MLIBs (**Table *2***). For instance, Fan *et al.* reported that the interlayer enlarged MoS_2/graphene composite (E−MG) could deliver an initial specific capacity of 320 mAh g^{-1} with a good cycling capacity of 290 mAh g^{-1} after 120 cycles [33]. Also, a comparable electrochemical performance was reported by Yu *et al.* when they applied various vdWHs in MLIBs namely, MoSSe/graphene (v−MoSSe/G) (350.8 mAh g^{-1}) [37] and MoS_2/graphene (MoS_2/G VH) (348.3 mAh g^{-1}) [42]. Among the reported MoS_2−composites, tin(IV) sulfide−molybdenum disulfide heterostructures (SnS_2−MoS_2) stand out as superior cathode material for MLIBs with an initial specific capacity of 1009 mAh g^{-1} as displayed in **Fig. *3*.b** [41]. Unfortunately, the exceptional specific capacity of SnS_2−MoS_2 sharply decreased to 600 mAh g^{-1} in the second cycle and stabilized at 450 mAh g^{-1} after 500 cycles. The excellent performance of SnS_2−MoS_2 was ascribed to the collaborative interaction between SnS_2 and MoS_2 in the heterostructure through multiple intercalation, conversion, and alloying reactions [41]. More specifically, MoS_2 played an important role in improving the structural integrity and cycling stability of SnS_2−MoS_2 by (I) providing adsorption sites for polysulfide byproducts, (II) allowing the rapid ion diffusion through its 1T−phase, and (III) preventing the aggregation of SnS_2 nanoparticles by permitting them to dispersedly grow on its nanosheets [41].

Many theoretical calculations elucidated that the Mg^{2+} intercalation in the interlayer spacing of MoS_2 requires a large activation energy of 2.61 eV [1]. In contrast, Li^+ ions need a lower activation energy of 0.49 eV [38]. Moreover, the charge density of Li^+ (54 C mm^{-3}) is much lower than that of Mg^{2+} (120 C mm^{-3} [41]. These features of Li^+ will favor the easy and fast insertion/extraction of Li^+ ions in/out of the interlayer spacing of MoS_2. Consequently, the reaction kinetics on the cathode side will greatly be enhanced. In addition, most of the articles tabulated in **Table *2*** mentioned that the Li^+ intercalation improves the electrochemical properties of MoS_2 by phase transformation of MoS_2 from 2H−phase to 1T−phase [1], [35], [40]. 1T−MoS_2 has higher electric conductivity (10−100 S cm^{-1}) than that of 2H−MoS_2 [41]. Thus, the phase transformation of MoS_2 during Li^+ intercalation will also enhance the electric conductivity of the electrode and reduce the charge transfer resistance [32], [33]. Furthermore, the pre−intercalation of Li^+ improves the ion diffusivity by deforming the layered structure of MoS_2, consequently, opening more channels for ion insertion, particularly Mg^{2+} [40].

5. CONCLUSIONS

This review article comprehensively discussed the development of various MoS_2−based cathode materials for RMBs and MLIBs. The literature review survey showed that MoS_2 prepared by Liang *et al.* [4] was the best pristine MoS_2 applied in RMBs with a specific capacity of 170 mAh g^{-1}. Also, several MoS_2−based composites were proposed in the literature as active cathode materials for RMBs. However, few composites exhibited a good electrochemical performance; for example, MoS_2/C [19], MoS_2/GR [21], and hydrous MoS_2 [29]. On the other hand, the performance of MoS_2−based materials in MLIBs is distinctively better than that of RMBs due to the rapid and easy intercalation/deintercalation of Li^+ ions in/out of MoS_2's interlayer spacing. The introduction of MLIBs opens a new door for promising, efficient, and highly safe multivalent rechargeable batteries.

6. ACKNOWLEDGMENT

This work is supported by the NEXT Center of Innovation Program (COI-NEXT) of the Japan Science and Technology Agency (Grant Number: JPMJPF2016).

7. REFERENCES

[1] Y. Ju *et al.*, "Li+/Mg2+ Hybrid-Ion Batteries with Long Cycle Life and High Rate Capability Employing MoS2 Nano Flowers as the Cathode Material," *Chem. Eur. J.*, vol. 22, no. 50, pp. 18073–18079, 2016.

[2] S. Chen, S. Fan, H. Li, Y. Shi, and H. Y. Yang, "Recent advances in kinetic optimizations of cathode materials for rechargeable magnesium batteries," *Coord. Chem. Rev.*, vol. 466, p. 214597, 2022, doi: https://doi.org/10.1016/j.ccr.2022.214597.

[3] X. Hou *et al.*, "Hollow opening nanoflowers MoS2-CuS-EG cathodes for high-performance hybrid Mg/Li-ion batteries," *Chem. Eng. J.*, vol. 409, p. 128271, 2021.

[4] Y. Liang, R. Feng, S. Yang, H. Ma, J. Liang, and J. Chen, "Rechargeable Mg Batteries with Graphene-like MoS2 Cathode and Ultrasmall Mg Nanoparticle Anode," *Adv. Mater.*, vol. 23, no. 5, pp. 640–643, Feb. 2011, doi: https://doi.org/10.1002/adma.201003560.

[5] C. Wu, G. Zhao, S. Gong, N. Zhang, and K. Sun, "PVP incorporated MoS 2 as a Mg ion host with enhanced capacity and durability," *J. Mater. Chem. A*, vol. 7, no. 9, pp. 4426–4430, 2019.

[6] M. Kotobuki, B. Yan, and L. Lu, "Recent progress on Cathode Materials for Rechargeable Magnesium Batteries," *Energy Storage Mater.*, 2022.

[7] M. Xu, N. Bai, H.-X. Li, C. Hu, J. Qi, and X.-B. Yan, "Synthesis of MXene-supported layered MoS2 with enhanced electrochemical performance for Mg batteries," *Chinese Chem. Lett.*, vol. 29, no. 8, pp. 1313–1316, 2018.

[8] Y. Liu, L.-Z. Fan, and L. Jiao, "Graphene intercalated in graphene-like MoS2: A promising cathode for rechargeable Mg batteries," *J. Power Sources*, vol. 340, pp. 104–110, 2017, doi: https://doi.org/10.1016/j.jpowsour.2016.11.060.

[9] K. Momma and F. Izumi, "VESTA 3 for three-dimensional visualization of crystal, volumetric and morphology data," *J. Appl. Crystallogr.*, vol. 44, no. 6, pp. 1272–1276, 2011.

[10] Z.-L. Tao, L.-N. Xu, X.-L. Gou, J. Chen, and H.-T. Yuan, "TiS 2 nanotubes as the cathode materials of Mg-ion batteries," *Chem. Commun.*, no. 18, pp. 2080–2081, 2004.

[11] X. Sun, V. Duffort, B. L. Mehdi, N. D. Browning, and L. F. Nazar, "Investigation of the mechanism of Mg insertion in birnessite in nonaqueous and aqueous rechargeable Mg-ion batteries," *Chem. Mater.*, vol. 28, no. 2, pp. 534–542, 2016.

[12] L. Jiao, H. Yuan, Y. Wang, J. Cao, and Y. Wang, "Mg intercalation properties into open-ended vanadium oxide nanotubes," *Electrochem. commun.*, vol. 7, no. 4, pp. 431–436, 2005.

[13] H. Xu *et al.*, "Rational design of high concentration electrolytes and MXene-based sulfur host materials toward high-performance magnesium sulfur batteries," *Chem. Eng. J.*, vol. 428, p. 131031, 2022.

[14] M. Pan *et al.*, "Using CoS cathode materials with 3D hierarchical porosity and an ionic liquid (IL) as an electrolyte additive for high capacity rechargeable magnesium batteries," *J. Mater. Chem. A*, vol. 7, no. 32, pp. 18880–18888, 2019.

[15] V. P. Hoang Huy, Y. N. Ahn, and J. Hur, "Recent advances in transition metal dichalcogenide cathode materials for aqueous rechargeable multivalent metal-ion batteries," *Nanomaterials*, vol. 11, no. 6, p. 1517, 2021.

[16] S. Yang, D. Li, T. Zhang, Z. Tao, and J. Chen, "First-Principles Study of Zigzag MoS2 Nanoribbon As a Promising Cathode Material for Rechargeable Mg Batteries," *J. Phys. Chem. C*, vol. 116, no. 1, pp. 1307–1312, Jan. 2012, doi: 10.1021/jp2097026.

[17] M. Asif, S. Kilian, and M. Rashad, "Uncovering electrochemistries of rechargeable magnesium-ion batteries at low and high temperatures," *Energy Storage Mater.*, vol. 42, pp. 129–144, 2021, doi: https://doi.org/10.1016/j.ensm.2021.07.031.

[18] X.-L. Li and Y.-D. Li, "MoS2 nanostructures: synthesis and electrochemical Mg2+ intercalation," *J. Phys. Chem. B*, vol. 108, no. 37, pp. 13893–13900, 2004.

[19] Y. Liu *et al.*, "Sandwich-structured graphene-like MoS 2/C microspheres for rechargeable Mg batteries," *J. Mater. Chem. A*, vol. 1, no. 19, pp. 5822–5826, 2013.

[20] Y. Liu *et al.*, "Synthesis of rGO-supported layered MoS 2 for high-performance rechargeable Mg batteries," *Nanoscale*, vol. 5, no. 20, pp. 9562–9567, 2013.

[21] C. Wu *et al.*, "MoS2/graphene heterostructure with facilitated Mg-diffusion kinetics for high-performance rechargeable magnesium batteries," *Chem. Eng. J.*, vol. 412, p. 128736, 2021.

[22] Y. Liang *et al.*, "Interlayer-expanded molybdenum disulfide nanocomposites for electrochemical magnesium storage," *Nano Lett.*, vol. 15, no. 3, pp. 2194–2202, 2015.

[23] R. Yokozaki, H. Kobayashi, T. Mandai, and I. Honma, "Effect of Al substitution on structure and cathode performance of MgMn2O4 spinel for magnesium rechargeable battery," *J. Alloys Compd.*, vol. 872, p. 159723, 2021, doi: https://doi.org/10.1016/j.jallcom.2021.159723.

[24] T. Mandai, A. Kutsuma, M. Konya, Y. Nakabayashi, and K. Kanamura, "Room temperature operation of magnesium rechargeable batteries with a hydrothermally treated ZnMnO3 defect spinel cathode," *Electrochemistry*, vol. 90, no. 2, p. 27005, 2022.

[25] S. Zhuo *et al.*, "Hierarchical Nanocapsules of Cu-Doped MoS2@H-Substituted Graphdiyne for Magnesium Storage," *ACS Nano*, vol. 16, no. 3, pp. 3955–3964, Mar. 2022, doi: 10.1021/acsnano.1c09405.

[26] G. Venkateswarlu, D. Madhu, and J. V. Rani, "Electroanalytical characterization of F-doped MoS2 cathode material for rechargeable magnesium battery," *Funct. Mater. Lett.*, vol. 12, no. 03, p. 1950041, 2019.

[27] F. Zhu, H. Zhang, Z. Lu, D. Kang, and L. Han, "Controlled defective engineering of MoS2 nanosheets for rechargeable Mg batteries," *J. Energy Storage*, vol. 42, p. 103046, 2021.

[28] K. W. Nam *et al.*, "The High Performance of Crystal Water Containing Manganese Birnessite Cathodes for Magnesium Batteries," *Nano Lett.*, vol. 15, no. 6, pp. 4071–4079, Jun. 2015, doi: 10.1021/acs.nanolett.5b01109.

[29] C. Wu *et al.*, "Interlayer-Expanded MoS2 Containing Structural Water with Enhanced Magnesium Diffusion Kinetics and Durability," *Chemelectrochem*, vol. 8, no. 23, pp. 4559–4563, 2021.

[30] X. Lin *et al.*, "General Liquid-Driven Coaxial Flow Focusing Preparation of Novel Microcapsules for Rechargeable Magnesium Batteries," *Adv. Sci.*, vol. 8, no. 2, p. 2002298, 2021.

[31] J. Liu, Y. Zhong, X. Li, T. Ying, T. Han, and J. Li, "A novel rose-with-thorn ternary MoS 2@ carbon@ polyaniline nanocomposite as a rechargeable magnesium battery cathode displaying stable capacity and low-temperature performance," *Nanoscale Adv.*, vol. 3, no. 19, pp. 5576–5580, 2021.

[32] C.-J. Hsu, C.-Y. Chou, C.-H. Yang, T.-C. Lee, and J.-K. Chang, "MoS 2/graphene cathodes for reversibly storing Mg 2+ and Mg 2+/Li+ in rechargeable magnesium-anode batteries," *Chem. Commun.*, vol. 52, no. 8, pp. 1701–1704, 2016.

[33] X. Fan, R. R. Gaddam, N. A. Kumar, and X. S. Zhao, "A hybrid Mg2+/Li+ battery based on interlayer-expanded MoS2/graphene cathode," *Adv. Energy Mater.*, vol. 7, no. 19, p. 1700317, 2017.

[34] Q. D. Truong *et al.*, "Exfoliated MoS2 and MoSe2 Nanosheets by a supercritical fluid process for a hybrid Mg–Li-ion battery," *ACS omega*, vol. 2, no. 5, pp. 2360–2367, 2017.

[35] Y. Tan *et al.*, "MoS2-Nanosheet-Decorated Carbon Nanofiber Composites Enable High-Performance Cathode Materials for Mg Batteries," *ChemElectroChem*, vol. 5, no. 7, pp. 996–1001, 2018.

[36] Q. Shu *et al.*, "MoS2-CuS-EG/carbon cloth Flexible cathode with Long-Cycling Life for Hybrid Mg-Li ion Batteries," *J. Alloys Compd.*, vol. 948, p. 169737, 2023.

[37] X. Yu *et al.*, "Constructing anion vacancy-rich MoSSe/G van der Waals heterostructures for high-performance Mg–Li hybrid-ion batteries," *J. Mater. Chem. A*, vol. 9, no. 40, pp. 23276–23285, 2021.

[38] X. Yu, G. Zhao, H. Huang, C. Liu, P. Lyu, and N. Zhang, "Interlayer-expanded MoS2 nanoflowers anchored on the graphene: A high-performance Li+/Mg2+ co-intercalation cathode material," *Chem. Eng. J.*, vol. 428, p. 131214, 2022.

[39] Z. Xiong *et al.*, "Hydrochloric Acid-Assisted Synthesis of Highly Dispersed MoS2 Nanoflowers as the Cathode Material for Mg-Li Batteries," *ACS Appl. Energy Mater.*, vol. 5, no. 5, pp. 6274–6281, 2022.

[40] B. Li *et al.*, "Li+ additive accelerated structural transformation of MoS2 cathodes for performance-enhancing rechargeable Mg2+ batteries," *Mater. Today Energy*, vol. 27, p. 101047, 2022.

[41] X. Fan, M. Tebyetekerwa, Y. Wu, R. R. Gaddam, and X. S. Zhao, "Magnesium/Lithium Hybrid Batteries

Based on SnS2-MoS2 with Reversible Conversion Reactions," *Energy Mater. Adv.*, 2022.

[42] X. Yu *et al.*, "A MoS2 and graphene alternately stacking van der Waals heterostructure for Li+/Mg2+ Co-intercalation," *Adv. Funct. Mater.*, vol. 31, no. 42, p. 2103214, 2021.